

Quality of Graphite Target for Biological/Biomedical/Environmental Applications of ^{14}C -Accelerator Mass Spectrometry

Seung-Hyun Kim,[†] Peter B. Kelly,[‡] Volkan Ortalan,[§] Nigel D. Browning,^{§,⊥} and Andrew J. Clifford^{*†}

Departments of Nutrition, Chemistry, and Chemical Engineering and Materials Science, University of California Davis, One Shields Avenue, Davis, California, 95616, and Condensed Matter and Materials Science Division, Lawrence Livermore National Laboratory, Livermore, California 94550

Catalytic graphitization for ^{14}C -accelerator mass spectrometry (^{14}C -AMS) produced various forms of elemental carbon. Our high-throughput Zn reduction method (C/Fe = 1:5, 500 °C, 3 h) produced the AMS target of graphite-coated iron powder (GCIP), a mix of non-graphitic carbon and Fe_3C . Crystallinity of the AMS targets of GCIP (nongraphitic carbon) was increased to turbostratic carbon by raising the C/Fe ratio from 1:5 to 1:1 and the graphitization temperature from 500 to 585 °C. The AMS target of GCIP containing turbostratic carbon had a large isotopic fractionation and a low AMS ion current. The AMS target of GCIP containing turbostratic carbon also yielded less accurate/precise ^{14}C -AMS measurements because of the lower graphitization yield and lower thermal conductivity that were caused by the higher C/Fe ratio of 1:1. On the other hand, the AMS target of GCIP containing non-graphitic carbon had higher graphitization yield and better thermal conductivity over the AMS target of GCIP containing turbostratic carbon due to optimal surface area provided by the iron powder. Finally, graphitization yield and thermal conductivity were stronger determinants (over graphite crystallinity) for accurate/precise/high-throughput biological, biomedical, and environmental ^{14}C -AMS applications such as absorption, distribution, metabolism, elimination (ADME), and physiologically based pharmacokinetics (PBPK) of nutrients, drugs, phytochemicals, and environmental chemicals.

Accelerator mass spectrometry (AMS) is the ultimate tool for ^{14}C tracer studies in vivo in a human for four reasons. First, AMS can measure $^{14}\text{C}/^{12}\text{C}$ ratios in the range of 10^{-12} – 10^{-16} . Second, ^{14}C has a low natural abundance ($^{14}\text{C}/^{12}\text{C}$ of 10^{-12}) and a long half-life (≈ 5730 yrs).^{1–3} Third, samples with one or less milligram carbon (mgC) can be analyzed by AMS. Fourth, AMS

throughput was only 5–10 min per sample for a precision of 1–5%. Thus, the amount of sample required for AMS and the sensitivity of AMS were each 3 orders of magnitude more sensitive than that for the liquid scintillation counter.^{1,4,5}

The ^{14}C -AMS application requires a special sample preparation protocol commonly called graphitization (conversion of carbonaceous samples to graphite or graphite-like materials).⁴ Graphite is soft and gray/black in color and is classified as natural and synthetic forms with different morphologies.^{6–8} Solid graphite or graphite-like materials were ideal for the ^{14}C -AMS, because they produced reliable ion current (C^-) with minimum sample to sample contamination. Furthermore, graphite can be handled in ambient level ^{14}C -AMS facilities because of its low vapor pressure. At the same time, precautions are necessary because graphite can absorb aerosol or vapor contaminants.⁹ Furthermore, graphite was the most popular form of carbon used in many industrial applications due to its thermal/chemical resistance and high electrical conductivity.^{6,7,10} Therefore, about 90% of carbon allotropes used in industries was of graphite or graphite-like materials.⁶

Graphitization methods for ^{14}C -AMS have been developed to accommodate microgram-sized carbonaceous samples, high throughput of sample preparation, minimum background effects, automate sample preparation, or all of the above.^{2,11–16}

- (1) Vogel, J. S.; Turteltaub, K. W.; Finkel, R.; Nelson, D. E. *Anal. Chem.* **1995**, *67*, 353A–359A.
- (2) Salehpour, M.; Possnert, G.; Bryhni, H. *Anal. Chem.* **2008**, *80*, 3515–3521.
- (3) Vogel, J. S.; Turteltaub, K. W. In *Mathematical Modeling in Experimental Nutrition*, AEMB 445; Clifford, A. J., Muller, H.-G., Eds.; Plenum Press: New York, 1998; pp 397–410.
- (4) Hellborg, R.; Skog, G. *Mass Spec. Rev.* **2008**, *27*, 398–427.
- (5) Vogel, J. S.; Love, A. H. *Methods Enzymol.* **2005**, 402–422.
- (6) Mochida, I.; Yoon, S. H.; Qiao, W. *J. Braz. Chem. Soc.* **2006**, *17*, 1059–1073.
- (7) Wissler, M. J. *Power Sources* **2006**, *156*, 142–150.
- (8) Kim, S. H.; Kelly, P. B.; Clifford, A. J. *Anal. Chem.* **2008**, *80*, 7661–7669.
- (9) Buchholz, B. A.; Freeman, S. P. H. T.; Haack, K. W.; Vogel, J. S. *Nucl. Instrum. Methods Phys. Res. Sect. B* **2000**, *172*, 404–408.
- (10) Oya, A.; Marsh, H. J. *Mater. Sci.* **1982**, *17*, 309–322.
- (11) Kim, S. H.; Kelly, P. B.; Clifford, A. J. *Anal. Chem.* **2008**, *80*, 7651–7660.
- (12) Xu, X.; Trumbore, S. E.; Zheng, S.; Southon, J. R.; McDuffee, K. E.; Luttgren, M.; Liu, J. C. *Nucl. Instrum. Methods Phys. Res. Sect. B* **2007**, *259*, 320–329.
- (13) Santos, G. M.; Southon, J. R.; Griffin, S.; Beaupre, S. R.; Druffel, E. R. M. *Nucl. Instrum. Methods Phys. Res. Sect. B* **2007**, *259*, 293–302.
- (14) Ognibene, T. J.; Bench, G.; Vogel, J. S.; Peaslee, G. F.; Murov, S. *Anal. Chem.* **2003**, *75*, 2192–2196.

* To whom correspondence should be addressed. E-mail: ajclifford@ucdavis.edu. Tel: 530-752-3376. Fax: 530-752-8966.

[†] Department of Nutrition, University of California Davis.

[‡] Department of Chemistry, University of California Davis.

[§] Department of Chemical Engineering and Materials Science, University of California Davis.

[⊥] Lawrence Livermore National Laboratory.

Iron, cobalt, or nickel catalysts were widely used for catalytic graphitization for ^{14}C -AMS applications such as radiocarbon dating or biological/biomedical/environmental studies^{17–19} as well as industrial purposes.^{6,7} Catalytic graphitization methods produced solid fullerene,⁵ amorphous carbon (a-C),¹⁹ or metal carbides (i.e., Fe_3C)^{8,15,18} as well as different morphological/structural graphite forms (i.e., fullerene graphite,¹⁴ filamentous graphite,²⁰ nanocrystalline graphitizable carbon (g-C)⁸). However, gaps in our knowledge of the relationships between graphite qualities of AMS targets and ^{14}C -AMS performance existed. Therefore, we characterized graphite qualities of AMS targets¹¹ and correlated graphite qualities with the sensitivity, accuracy, and precision of ^{14}C -AMS measurement. Graphite qualities, in the present study, were described as isotopic fractionation during the graphitization steps, graphitization yield, crystal size, and crystallinity. Furthermore, robust ion currents ($^{12}\text{C}^-$, $^{13}\text{C}^+$, and normalized $^{13}\text{C}^+$) were required for high-throughput (HT), accurate, and precise ^{14}C -AMS performances. Because ^{14}C -AMS is the ultimate tool for ^{14}C tracer studies in vivo human, it was important to fill the gaps that existed in our knowledge of the relationships between graphite qualities of AMS targets and ^{14}C -AMS performance for quantifying the in vivo human absorption, distribution, metabolism, elimination (ADME), and physiologically based pharmacokinetics (PBPK) of nutrients, drugs, phytochemicals, and environmental chemicals.

EXPERIMENTAL SECTION

Reagents. All reagents and supplies used in present study were as previously described.^{8,11,21} The oxalic acid II (Ox-2, $\text{C}_2\text{H}_2\text{O}_4$, NIST SRM 4990C) which contained one milligram carbon (mgC) was commonly used as the AMS standard. The Ox-2 and/or synthetic graphite standard (GST, CAS # 7782–42–5, Sigma-Aldrich) were used as carbonaceous test samples, which were graphitized for ^{14}C -AMS measurement using our high-throughput (HT) Zn reduction method.¹¹ The graphitized carbonaceous test samples were also used for quantifying the isotopic fractionation and graphitization yield, as well as for characterizing the visual and structural traits.

Procedures. After graphitization,¹¹ the carbonaceous test samples were converted to graphite-coated Fe powder (GCIP), graphite-coated Fe (GCI), or iron–carbon material (ICM) which was referred to as AMS targets. Our AMS targets of ICM, GCI, and GCIP were a mix of g-C and/or iron carbide (mostly, Fe_3C) with a different ratio of g-C and Fe_3C .⁸

Four graphitization temperatures and four mass ratios of carbon and Fe (C/Fe) were tested to investigate graphite qualities (i.e., isotopic fractionation during the graphitization steps, graphi-

tization yield, crystal size, crystallinity) of our AMS targets and ^{14}C -AMS performances (i.e., ion currents, accuracy and precision of isotope ratio measurement). The graphitization temperatures were tested at 400, 500, 525, and 585 °C. The C/Fe (w:w) was tested in the ratios of 1:1, 1:5, 1:10, and 1:15. All of the other graphitization conditions except for the C/Fe ratios and graphitization temperatures were the same as previously described.¹¹

Visual/structural traits of our AMS targets were investigated using a scanning electron microscope (SEM), a high resolution transmission electron microscope (HRTEM), X-ray diffraction (XRD), and a Raman spectrometer. All instrumental methods including sample preparations were as previously described except for TEM.^{8,11}

For HRTEM measurements, we used only the AMS targets of GCIP that were prepared using two different conditions (C/Fe = 1:5, 500 °C, 3 h¹¹ versus C/Fe = 1:1, 585 °C, 3 h). These AMS targets of GCIP were prepared by dipping a Lacey carbon (i.e., a-C) coated Cu-grid into the powder. In our experience, grinding and sonication of these AMS targets of GCIP caused the carbon shell to be separate from a carbon-encapsulated Fe (C-Fe). The HRTEM experiments were performed on a field emission gun JEOL (S)TEM instrument (JEM2500SE) operated at 200 kV. Compositional analyses were performed by electron energy loss spectrum (EELS) with a postcolumn Gatan imaging filter. For high angle annular dark field-scanning transmission electron microscopy (HAADF-STEM) experiments, a nominal 1 nm spot size was used with an 800 mm camera length, corresponding to an inner–outer semicollection angle of 35 and 100 mrad, respectively.

Graphitization yield (%) and isotopic fractionation ($\delta^{13}\text{C}$, ‰) were measured with a PDZ Europa ANCA-GSL elemental analyzer interfaced to a PDZ Europa 20-20 isotope ratio mass spectrometer (EA-IRMS, Sercon Ltd., Cheshire, UK).²² The consensus $\delta^{13}\text{C}$ of the Ox-2 was $-17.8 \pm 0.05\text{‰}$.²³ The ^{14}C level (Fraction Modern, F_m) of carbonaceous test samples was measured with the AMS.¹¹ One F_m is equal to 97.9 attomole ^{14}C /mgC or 6.11 femto curies/mgC, and the atmospheric F_m in 2007 was ≈ 1.05 . The accepted/certified F_m of the Ox-2 is 1.3407.²³

Terminology such as graphitic, nongraphitic, graphitizable (g-C), nongraphitizable, or turbostratic (T_s) carbon used for the characterization of the AMS targets is defined in previous publications (see Supporting Information, Figure S1).²⁴

RESULTS

The SEM images of AMS targets of ICM, GCI, and GCIP (Figure 1) depended on (two-way) interaction between C/Fe ratio and CO_2 reduction temperature. The CO_2 from the combustion step of a sample of interest was converted to graphite, graphite-like materials, and/or Fe_3C . Graphite deposition was not observed when the C/Fe ratio was 1:1–1:15 at 400 °C. Only visual change/deformation of the –400 mesh spherical iron powder surface (–400MSIP, $<37\ \mu\text{m}$, CAS #7439–89–6, Sigma-Aldrich) was observed (Figure 1). The AMS targets in all C/Fe ratios at 400 °C appeared as ICM. The carbon deposition was observed in all C/Fe ratios at 500–585 °C. The AMS targets

(15) Vogel, J. S. *Radiocarbon* **1992**, *34*, 344–350.

(16) Ramsey, C. B.; Hedges, R. E. M. *Nucl. Instrum. Methods Phys. Res. Sect. B* **1997**, *123*, 539–545.

(17) Vogel, J. S.; Southon, J. R.; Nelson, D. E. *Nucl. Instrum. Methods Phys. Res. Sect. B* **1987**, *29*, 50–56.

(18) Jull, A. J. T.; Donahue, D. J.; Hatheway, A. L.; Linick, T. W.; Toolin, L. J. *Radiocarbon* **1986**, *28*, 191–197.

(19) Vogel, J. S.; Southon, J. R.; Nelson, D. E.; Brown, T. A. *Nucl. Instrum. Methods Phys. Res. Sect. B* **1984**, *5*, 289–293.

(20) Santos, G. M.; Mazon, M.; Southon, J. R.; Rifai, S.; Moore, R. *Nucl. Instrum. Methods Phys. Res. Sect. B* **2007**, *259*, 308–315.

(21) Getachew, G.; Kim, S. H.; Burri, B. J.; Kelly, P. B.; Haack, K. W.; Ognibene, T. J.; Buchholz, B. A.; Vogel, J. S.; Modrow, J.; Clifford, A. J. *Radiocarbon* **2006**, *48*, 325–336.

(22) Kim, S. H.; Kelly, P. B.; Clifford, A. J. *Anal. Chem.* **2009**, *81*, 5949–5954.

(23) Mann, W. B. *Radiocarbon* **1983**, *25*, 519–527.

(24) McNaught, A. D.; Wilkinson, A. *IUPAC Compendium of Chemical Terminology*; Blackwell Science Ltd.: Malden, MA, 1997.

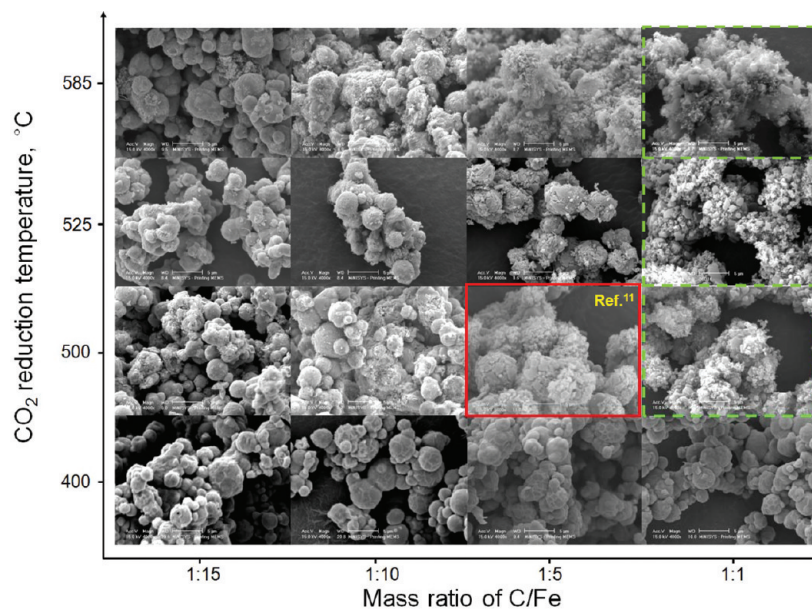


Figure 1. Scanning electron microscope (SEM) images of the AMS targets depended on the (two-way) interaction between the C/Fe ratio and the CO_2 reduction temperatures. The rectangle within the solid red border (C/Fe ratio of 1:5 and reduction temperature of $500\text{ }^\circ\text{C}^{11}$) was an AMS target of GCIP that consisted of a mix of a graphite sheet carbon and a fuzz carbon. As the C/Fe ratio was raised from 1:5 to 1:1 and reduction temperatures were raised from 500 to 525 $^\circ\text{C}$ and to 585 $^\circ\text{C}$ (rectangles within the broken green borders), much more carbon sheet and more fuzz carbon were produced in the AMS targets of GCIP.

appeared as GCIP in the C/Fe ratios of 1:1–1:5 at 500–585 $^\circ\text{C}$ or as GCI with C/Fe ratios of 1:10–1:15 at 500–585 $^\circ\text{C}$. The AMS targets of GCIP had a uniform carbon deposition, more fuzz (coated on the surface of Fe catalyst adhered more strongly than the covered “fluff”¹¹ and more carbon/or graphite sheets than the AMS targets of GCI. The AMS targets of GCIP with C/Fe ratio of 1:1 at 500–585 $^\circ\text{C}$ (broken green borders) were visually observed with more fuzz and more carbon/or graphite sheets over the AMS target of GCIP using our HT Zn reduction method¹¹ (solid red border, C/Fe = 1:5, 500 $^\circ\text{C}$).

Figure 2 summarized XRD spectra of AMS targets of ICM, GCI, and GCIP that depended on (the two-way) interaction between C/Fe ratio and CO_2 reduction temperature. The AMS targets of ICM with C/Fe ratios of 1:1–1:15 at 400 $^\circ\text{C}$ did not show the graphite reflection peak (G-002) at 2θ of $\approx 26^\circ$. The few/weak Fe_3C peaks were detected at 2θ of 30–75 $^\circ$.

The AMS targets of GCI and GCIP with C/Fe ratios of 1:5–1:15 at 500–585 $^\circ\text{C}$ did not show the G-002 at 2θ of $\approx 26^\circ$. However, AMS targets of GCIP with C/Fe ratio of 1:1 at 500 $^\circ\text{C}$ and at 525 $^\circ\text{C}$ were observed to have weak/broad G-002 peaks at 2θ of 25–28 $^\circ$. Because the AMS targets of GCIP with C/Fe ratio of 1:1 at 500–525 $^\circ\text{C}$ had disordered (/or less-ordered)-nanocrystalline graphite, their crystal size (stacking height, L_c) and interlayer distance (d_{002}) were not measurable. While, the AMS target of GCIP with C/Fe ratio of 1:1 at 585 $^\circ\text{C}$ had a slightly more intense G-002 peak at 2θ of $\approx 26.7^\circ$ (solid red circle in top right panel) and partially ordered-nanocrystalline graphite whose L_c was ≈ 5 nm and d_{002} was ≈ 0.335 nm. The Fe_3C peaks were detected at 2θ of 30–75 $^\circ$ in AMS targets of GCI and GCIP (C/Fe ratios of 1:1–1:15, 500–585 $^\circ\text{C}$).

Figure 3 summarized Raman spectra of the GST⁸ (Figure 3a), the AMS target of GCIP with C/Fe ratio of 1:5 at 500 $^\circ\text{C}^{11}$ (Figure 3b) and the AMS targets of GCIP with C/Fe ratio of 1:1 at 500 $^\circ\text{C}$ (Figure 3c), 525 $^\circ\text{C}$ (Figure 3d), and 585 $^\circ\text{C}$ (Figure 3e).

The GST (Figure 3a) is synthetic graphite, and its Raman spectrum showed a weak D band at 1339 cm^{-1} and an intense G band at 1566 cm^{-1} , both bands reflect first order Raman scatters. The GST also had an intense G' band at 2705 cm^{-1} and a weak D' band at 3229 cm^{-1} , both bands reflect second order Raman scatters. In-plane crystal sizes (L_a) of the GST were 37.9 nm as determined by the ratio of the intensities of D and G bands.⁸

The AMS target of GCIP, C/Fe ratio of 1:5 and 500 $^\circ\text{C}^{11}$ (Figure 3b) showed intense/broad D band at $\approx 1350\text{ cm}^{-1}$ and G band at $\approx 1580\text{ cm}^{-1}$. The L_a of this GCIP was 4.4 nm, and the L_c of this GCIP was not measurable due to its small size graphite crystallite, lack of stacking sequence/order, or both (Figure 3b). Full width half-maximum (fwhm) of D and G bands in the AMS target of GCIP in Figure 3b were 2 to 3 times broader than those in the GST⁸ (Figure 3a).

The AMS targets of GCIP (Figure 3c–e), C/Fe ratio of 1:1, and three different temperatures, were chosen to investigate the difference of graphite crystallinity, because the G-002 peaks were only found in these AMS targets of GCIP using XRD (Figure 2). Raman spectra of these AMS targets of GCIP (Figure 3c–e) also had broad D and G bands. The intensity ratio of D and G bands (I_D/I_G) in these AMS targets of GCIP (Figure 3c–e) became larger as CO_2 reduction temperatures increased from 500 to 585 $^\circ\text{C}$, indicating a small L_a (Figure 3). In general, the I_D/I_G was large due to minute size graphite crystallite, some a-C, or both.^{25,26} Furthermore, the faster growth of graphite crystal associated with the higher temperatures may have increased the number of defects in the nanocrystalline graphite while still producing larger crystals (3D direction), as suggested in a prior study.²⁷ The FWHMs of D and G bands (Figure 3c–e) were also

(25) Liu, T.-C.; Li, Y.-Y. *Carbon* **2006**, *44*, 2045–2050.

(26) Lu, Y.; Zhu, Z.; Liu, Z. *Carbon* **2005**, *43*, 369–374.

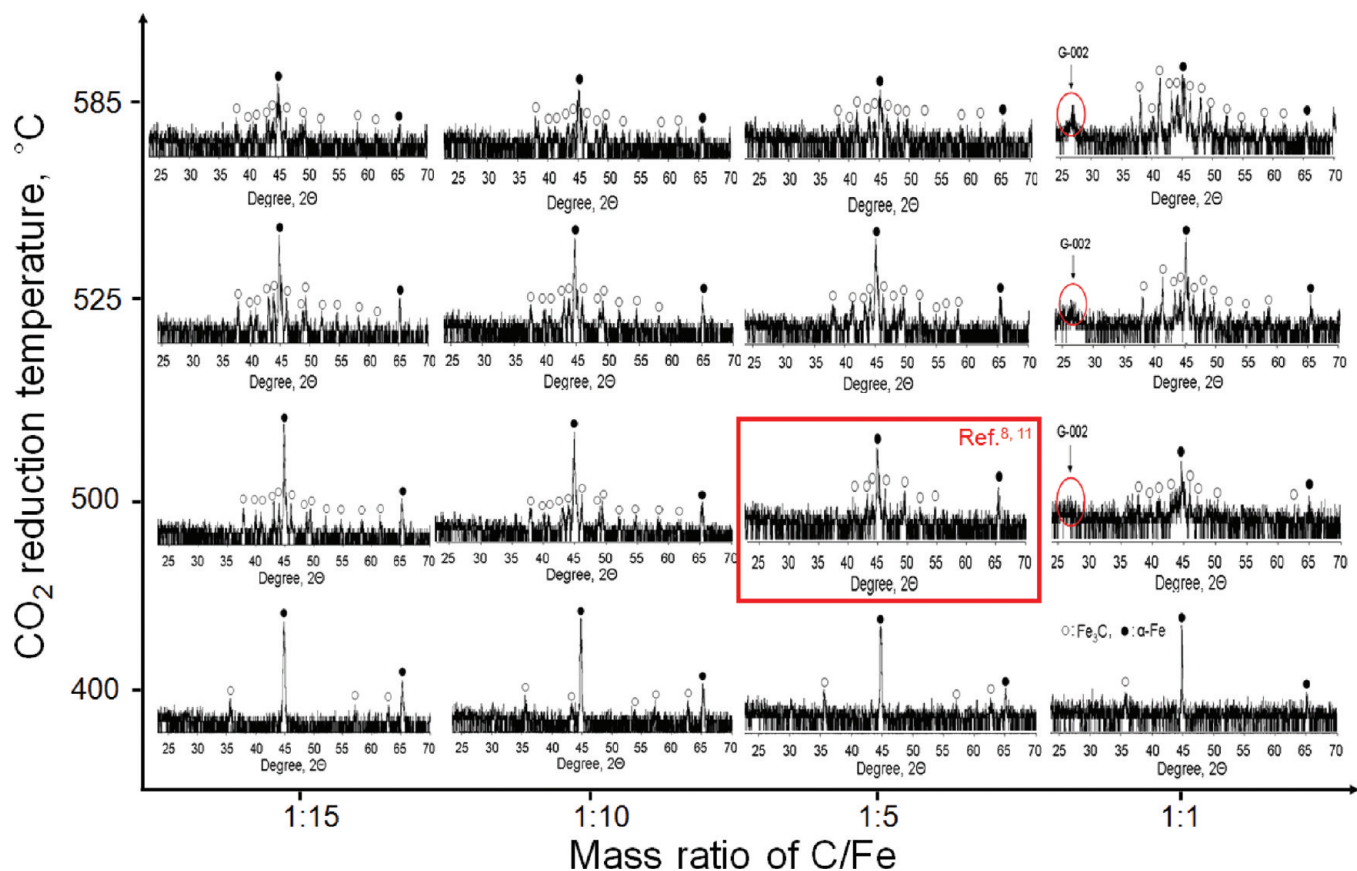


Figure 2. X-ray diffraction (XRD) spectra of the AMS targets varied with the C/Fe ratio and the CO₂ reduction temperatures. The AMS target of ICM¹¹ was produced using C/Fe ratios that ranged from 1:1 to 1:15 and 400 °C. The AMS target of ICM did not show the graphite reflection peak (G-002) at 2θ of ≈26°. Only a few weak Fe₃C peaks were detected at 2θ of 30–75° when a CO₂ reduction temperature of 400 °C was used. The AMS target of GCIP¹¹ was prepared with a C/Fe ratio of 1:5 and a reduction temperature of 500 °C. Its XRD spectrum was indicated by the rectangle within the solid red border. The AMS target of GCIP¹¹ showed an XRD spectrum with a measurable Fe₃C peak in the 2θ range of 30 to 75° but without a measurable G-002 peak. The graphite crystallinity (L_c , d_{002}) also depended on the C/Fe ratio and the CO₂ reduction temperature. When the C/Fe ratio was 1:1, raising the temperature from 500 to 525 °C to 585 °C raised the L_c of ≈5 nm and the d_{002} of ≈0.335 nm for the 1 mgC sized sample.

decreased by 21–41% when CO₂ reduction temperatures were increased from 500 to 585 °C. The AMS targets of GCIP (Figure 3c–e) still had very broad/weak second order Raman peaks which suggested less-ordered- or disordered-nanocrystalline graphite in the AMS targets of GCIP. The intensities of second order Raman peaks were greatest in the AMS target of GCIP with C/Fe ratio of 1:1 at 585 °C, indicating a more defined graphitic structure associated with the higher processing temperature.

Our overall schematic of graphite formation and understanding of carbon structure formation/transformation with various C/Fe ratios, CO₂ reduction temperatures, and/or heat treatment temperature (HTT, broken red lines) without catalyst activity were summarized in Figure 4. The CO₂ and H₂O from sample of interest were reduced to CO and H₂ by oxidation of Zn dust. The CO₂ and/or CO were the first formed iron carbides (especially, Fe₃C). Then, the Fe particle saturated with Fe₃C begins to reduce the graphite or graphite-like materials over the particle surface (Figure 4a).

Crystallinity of graphite/graphite-like materials was associated with graphitization conditions C/Fe ratio and CO₂ reduction

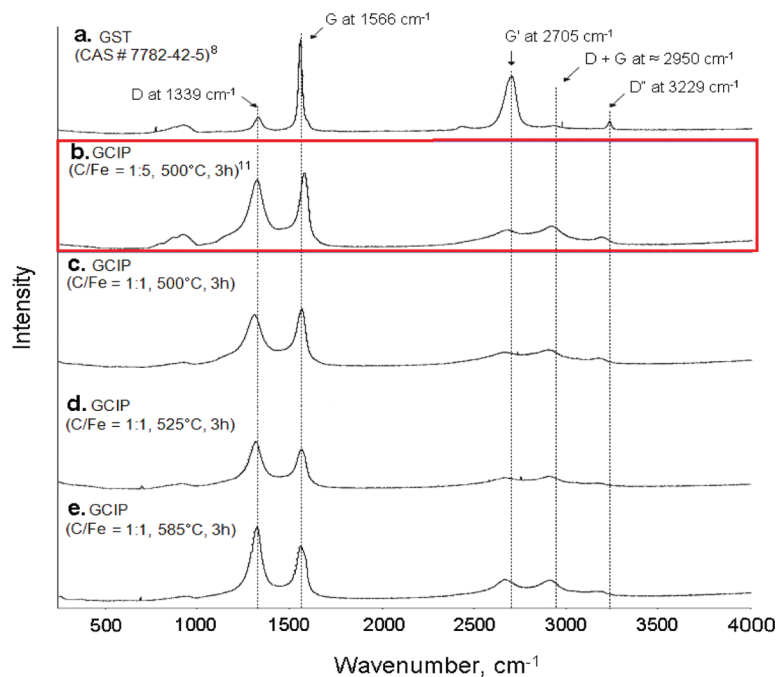
temperature. Nongraphitic carbon, consisted of nanocrystalline graphite, was produced on the iron carbide surface with C/Fe ratios of 1:1–1:15 (≥500 °C) (Figure 4b). Crystallinity of graphite/graphite-like materials was increased at higher CO₂ reduction temperature as the C/Fe ratio increased. Turbostratic carbon (T_s carbon) was directly produced with a C/Fe ratio of 1:1 at 585 °C. The Fe₃C or g-C would be transformed to T_s carbon at ≥1000 °C, microcrystalline carbon at >2000 °C, or graphite material at >2500 °C by the HTT (broken red lines, Figure 4b).

HRTEM was used to characterize and confirm morphology and crystalline structure of two GCIPs. One was produced with our HT Zn reduction method.¹¹ The other was produced with the same method,¹¹ except for using C/Fe ratio of 1:1 at 585 °C (Figure 5).

In left panels (Figure 5a–d), the AMS target of GCIP produced with our HT Zn reduction method¹¹ contained carbon sheets and carbon-encapsulated Fe (C-Fe). Carbon sheets were mostly a-C and had partially ordered and less-ordered nanocrystalline graphite

(27) Sergiienko, R.; Shibata, E.; Kim, S. H.; Kinota, T.; Nakamura, T. *Carbon* **2009**, *47*, 1056–1065.

(28) Yaguchi, T.; Sato, T.; Kamino, T.; Motomiya, K.; Tohji, K.; Kasuya, A. *Microsc. Microanal.* **2002**, *8*, 1152CD–1153CD.



Samples, $n \geq 6$	Full width half maximum (FWHM), cm^{-1}		I_D/I_G	In-plane crystal size, L_a^{36} , nm
	D band	G band		
a. GST (CAS # 7782-42-5) ⁸	43 ± 3.5^a	21 ± 1.4^a	0.12 ± 0.03^a	37.9 ± 8.1^a
b. GCIP (C/Fe = 1:5, 500°C, 3h) ¹¹	98 ± 7.7^b	66 ± 7.2^b	1.01 ± 0.09^b	4.4 ± 0.4^b
c. GCIP (C/Fe = 1:1, 500°C, 3h)	121 ± 7.3^c	84 ± 12.6^c	1.03 ± 0.07^b	4.3 ± 0.3^b
d. GCIP (C/Fe = 1:1, 525°C, 3h)	92 ± 2.7^d	70 ± 2.7^b	1.21 ± 0.03^c	3.6 ± 0.1^b
e. GCIP (C/Fe = 1:1, 585°C, 3h)	71 ± 1.2^e	66 ± 2.5^b	1.43 ± 0.04^d	3.1 ± 0.1^c
P-value	< 0.0001	< 0.001	< 0.0001	< 0.0001

Figure 3. Raman spectra of GST, CAS # 7782-42-5, (a) and the AMS target of GCIP using C/Fe ratio of 1:5 at 500 °C for 3 h¹¹ (b, within solid red rectangle). The remaining AMS targets of GCIP used C/Fe ratio of 1:1 at 500 °C for 3 h (c), 525 °C for 3 h (d), and 585 °C for 3 h (e). In-plane crystal sizes (L_a) were calculated as $L_a = C/(I_D/I_G)$, where C was ≈ 4.4 nm.³⁶ L_a was inversely correlated with I_D/I_G ($R = -0.952$, $P = 0.0088$). (a–e) Values with different superscripts differed from one another ($P < 0.0001$).

(Figure 5a). In the C-Fe, carbon shell (or layer) was graphite sheet ($d_{002} = 0.344$ nm) that included partial stacking sequence defects. Carbon shell thickness in the C-Fe was 4.9 nm (Figure 5b). Scanning transmission electron microscopy-electron energy loss spectrum (STEM-EELS) showed ordered and semioordered graphite. The STEM-EELS of graphite or graphitic carbon showed sharp and strong π^* and σ^* peaks, while STEM-EELS of a-C showed very broad and strong σ^* peaks (very weak π^* peak). The STEM-EELS in the AMS target of GCIP produced with our HT Zn reduction method¹¹ were consistent with those of graphite and a-C in a previous study²⁸ (Figure 5c). The Fe_3C was also observed to be about 3 nm depth (but not uniform) into the Fe particle (Figure 5d).

In right panels (Figure 5e–h), the AMS target of GCIP with C/Fe ratio of 1:1 at 585 °C also had carbon sheets and C-Fe. The carbon sheets appeared as ribbon-like graphite which was ordered graphite ($d_{002} = 0.342$ nm), and graphite sheet thickness was 6.7 nm (Figure 5e). Carbon shell in the C-Fe was 10.7 nm, and it was a-C or nanocrystalline graphite with some crystalline and stacking sequence defects (Figure 5f). Crystalline and stacking sequence defects in the carbon shell were also confirmed with

STEM-EELS (Figure 5g). The Fe_3C appeared to interface with about 5 nm depths (but also not uniform) into the Fe particle (Figure 5h).

Finally, additional HRTEM images and diffraction patterns (that characterized Fe and Fe_3C) of the above two AMS targets of GCIP are available in the Supporting Information (Figure S2).

Figure 6 compared isotopic fractionation ($\delta^{13}\text{C}$), graphitization yield, and ^{14}C -AMS measurements (ion currents, F_m) of two AMS targets of GCIP (as in Figure 5) with different graphite crystallinity. Although the AMS target of GCIP (T_s carbon, C/Fe ratio of 1:1, 585 °C, 3 h) had more ordered nanocrystalline graphite ($L_c \approx 5$ nm in Figure 2), it showed an $\approx 0.7\%$ lighter $\delta^{13}\text{C}$ shift (Figure 6a) and 9% lower graphitization yield (Figure 6b) compared to those of the AMS target of GCIP (nongraphitic carbon^{8,11}) ($P < 0.0001$). Although differences of F_m between the AMS targets of GCIP (T_s carbon) and GCIP (nongraphitic carbon) were not significant ($P < 0.9804$), the AMS target of GCIP (T_s carbon) had less accurate and precise F_m value (relative error of 0.57%) than the AMS target of GCIP (nongraphitic carbon,^{8,11} relative error of -0.02%) (Figure 6c). In addition, the AMS target of GCIP (T_s carbon) produced an $\approx 40\%$

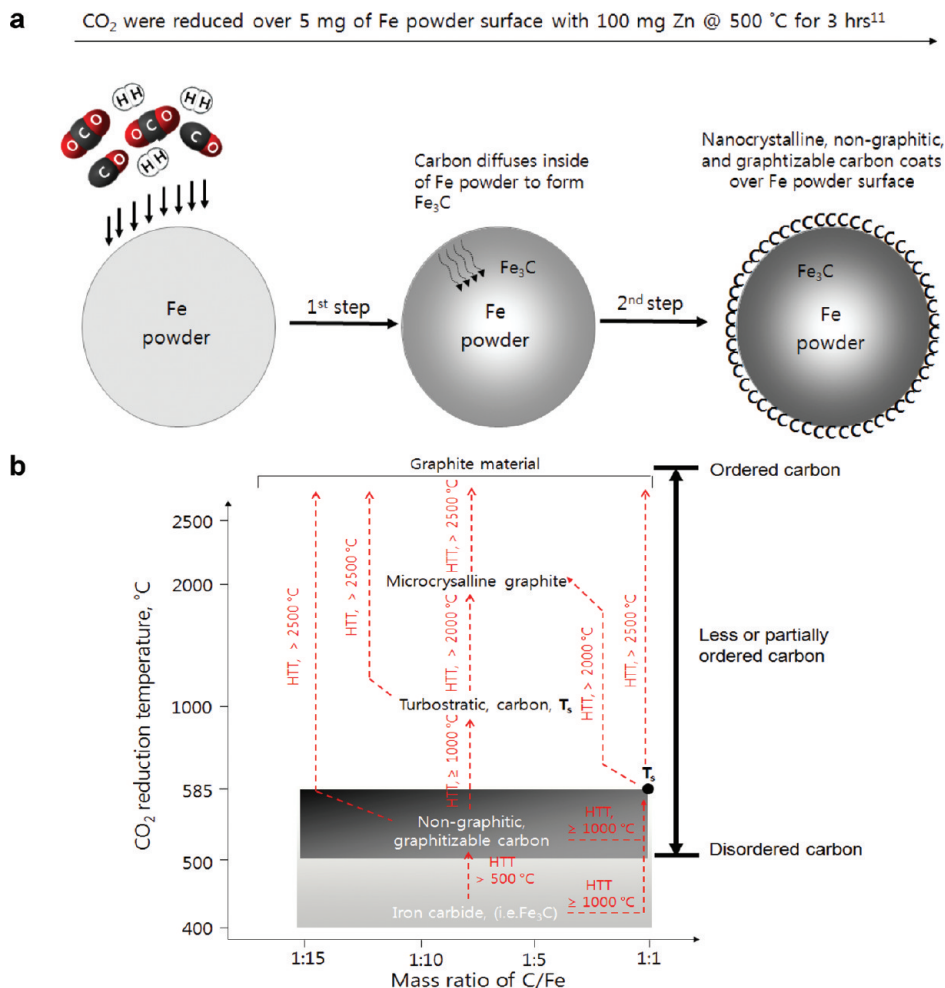


Figure 4. A model of graphite formation (a) and the carbon formations and transformations that may have occurred during graphitization using H_2 or Zn dust as reductants (b). Initially, CO_2 and/or CO were converted to iron carbides (especially, Fe_3C) that saturated the surface of the iron particle. Then, graphite or graphite-like materials were produced on the iron carbide surface (a). The iron carbide may have acted as the catalyst for formation of graphite. The crystallinity of graphite and/or graphite-like materials increased as the C/Fe ratio increased and the CO_2 reduction temperature increased, so that T_s carbon was produced directly with the C/Fe ratio of 1:1 at 585 °C for 3 h. Graphite material can be produced with the C/Fe ratio of 1:1 at >2500 °C. Furthermore, T_s can be produced from the nongraphitic carbon or Fe_3C by HTT (broken red lines). Finally, graphite material was also produced by heat treatment temperature (HTT, >2500 °C) alone from the nongraphitic, T_s carbon, or microcrystalline carbon (broken red lines).

lower $^{12}\text{C}^-$, $^{13}\text{C}^+$, and normalized $^{13}\text{C}^+$ ($n^{13}\text{C}^+$) currents ($P < 0.0001$) than the AMS target of GCIP (nongraphitic carbon^{8,11}) (Figure 6d–f).

DISCUSSION

^{14}C -AMS is the ultimate tool for ^{14}C tracer studies in vivo human, so the gaps in our knowledge of the relationships between graphite quality (i.e., isotopic fractionation during the graphitization steps, graphitization yield, crystal size, crystallinity) of AMS targets and the ^{14}C -AMS performance (i.e., ion currents, accuracy and precision of isotope ratio measurement) need to be filled. A complete understanding of the important parameters was important for accurate/precise/HT ^{14}C -AMS measurements in order to quantify the in vivo human ADME and PBPK of nutrients, drugs, phytochemicals, and environmental chemicals.

AMS graphite target was commonly prepared at 450–650 °C,^{2,12–14,19,29} the thermodynamically favored temperature for graphite formation.^{11,29} The graphite formation reactions were faster as temperature was raised.²⁹ Temperature dependence of

graphitization was detailed in the Supporting Information (Figure S3). Additional information on the effects of graphite crystallinity for accurate/precise/HT ^{14}C -AMS measurement was also included in the Supporting Information (Figure S4).

Characterization of AMS Targets versus Graphitization

Conditions. Although prior reports have characterized AMS targets as containing graphite,¹⁵ solid fullerene,⁵ a-C,¹⁹ or a fullerene “graphite”¹⁴, their visual appearances were not described. Visual comparison and/or confirmation of carbon deposition in AMS targets were evident with SEM, even though SEM images (SEMs) alone could not differentiate carbon allotrope structures. The AMS target of GCIP¹¹ (solid red border, Figure 1) was previously referred to as a mix of g-C and Fe_3C .⁸ The AMS targets of GCIP (broken green borders, Figure 1) appeared as a mix of carbon sheets and fuzz carbons. These carbon sheets were visually similar to the GST.⁸ However, fuzz carbons in the AMS targets of GCIP (broken green borders) differed from filamentous carbon, i.e. filamentous carbon had

(29) Verkouteren, R. M.; Klouda, G. A. *Radiocarbon* **1992**, *34*, 335–343.

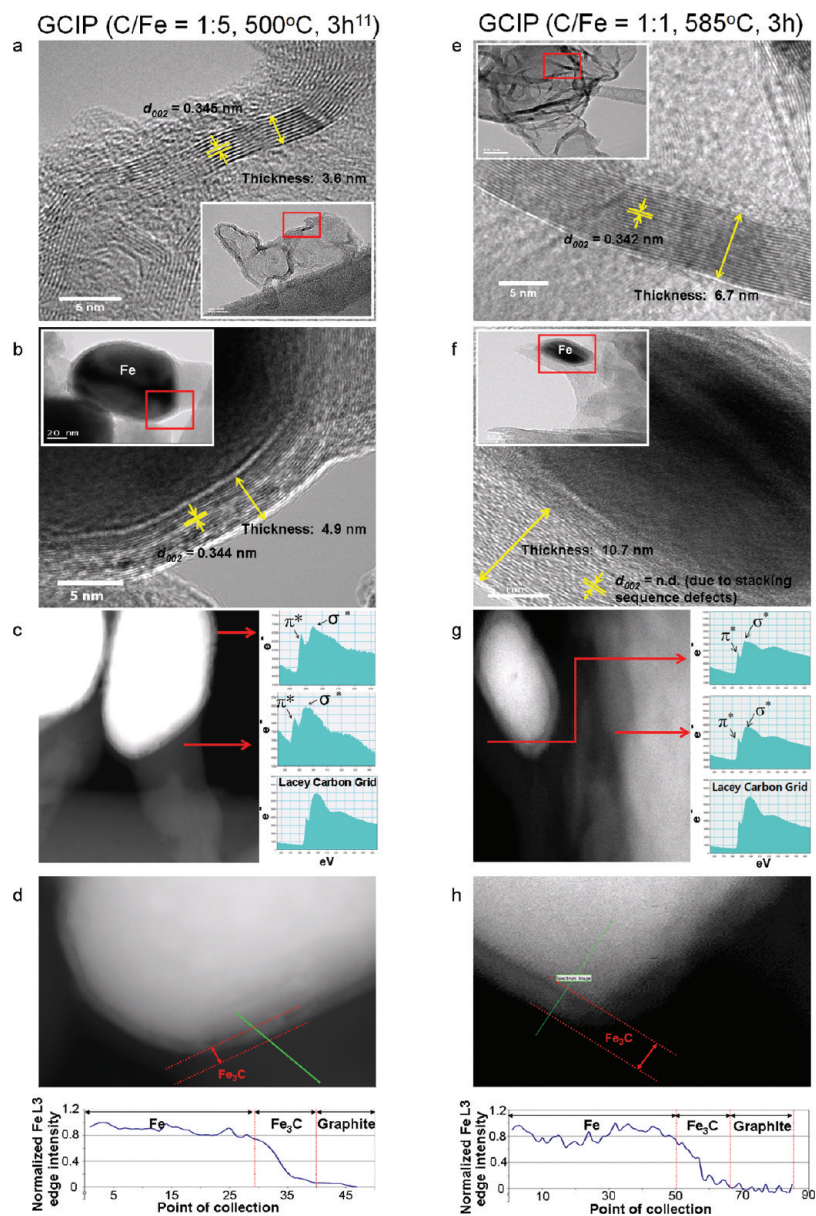


Figure 5. Comparison of HRTEM measurements of the AMS target of GCIP¹¹ and the AMS target of GCIP (C/Fe = 1:1, 585 °C, 3 h). Both AMS targets of GCIP consisted of carbon (/or graphite) sheet (a and e) and the carbon-encapsulated Fe (C-Fe, b and f). Enlarged images of the carbon sheet (a and e) and the C-Fe (b and f) matched the red rectangle area in each insert TEM image. The carbon sheet in the AMS target of GCIP (C/Fe = 1:1, 585 °C, 3 h) was more ordered ($d_{002} = 0.342$ nm) and thicker (6.7 nm) than that of the AMS target of GCIP¹¹ (a and e). The carbon shell in the AMS target of GCIP (C/Fe = 1:1, 585 °C, 3 h) was thicker (10.7 nm) than that in the AMS target of GCIP¹¹ (4.9 nm). However, the carbon shell in the AMS target of GCIP (C/Fe = 1:1, 585 °C, 3 h) was a less ordered carbon (b and f) compared to that in the AMS target of GCIP.¹¹ Although all graphitization processes were conducted under identical conditions, carbon shell thickness in the AMS target of GCIP was variable, because our Fe particle size was not uniform. STEM-EELS showed ordered, semioordered, and amorphous carbons in both AMS targets of GCIP. The EELS of both AMS targets of GCIP were consistent for those of graphite and a-C in a prior study²⁸ (c and g). The STEM-EELS line scan was performed to check the Fe composition along the C-Fe interface, along the green line (d and h). The distance between each spectrum was about 0.3 nm, and it was normalized to the FeL3 intensity along the green line. Even though the Fe₃C in the C-Fe was not uniform, it was detected by ≈ 5 nm deep into the Fe particle.

longer and more fibrous carbon structures.²⁰ Visual differences among AMS targets were associated with catalyst shape, type, particle size, graphitization temperature, time, and/or C/Fe ratio.^{8,20} Using our HT Zn reduction method,¹¹ in the present study, -400MSIP produced a powdery/soft AMS target of GCIP which was suitable for accurate/precise/HT ¹⁴C-AMS measurement because it had less sinter, high graphitization yield, high ion currents, and low $\delta^{13}\text{C}$ shift. In contrast, a prior study with different graphitization conditions²⁰ reported that -400MSIP

produced a solid/hard AMS target which was not optimal for ¹⁴C-AMS measurement due to sintering and hardness.

XRD measurements provided structural information such as crystallinity (stacking sequence, 3D) and/or crystalline defect in the graphite material. Graphite material had four reflection peaks (G-002, G-100, G-101, G-004) in 2θ of 25 to 55°.³⁰ The G-002 at 2θ of $\approx 26^\circ$ was used as a diagnostic peak for graphite material due to its strong/sharp intensity. The G-002 was weak/broad when graphite material had crystalline defects, less-ordered minute graphite crys-

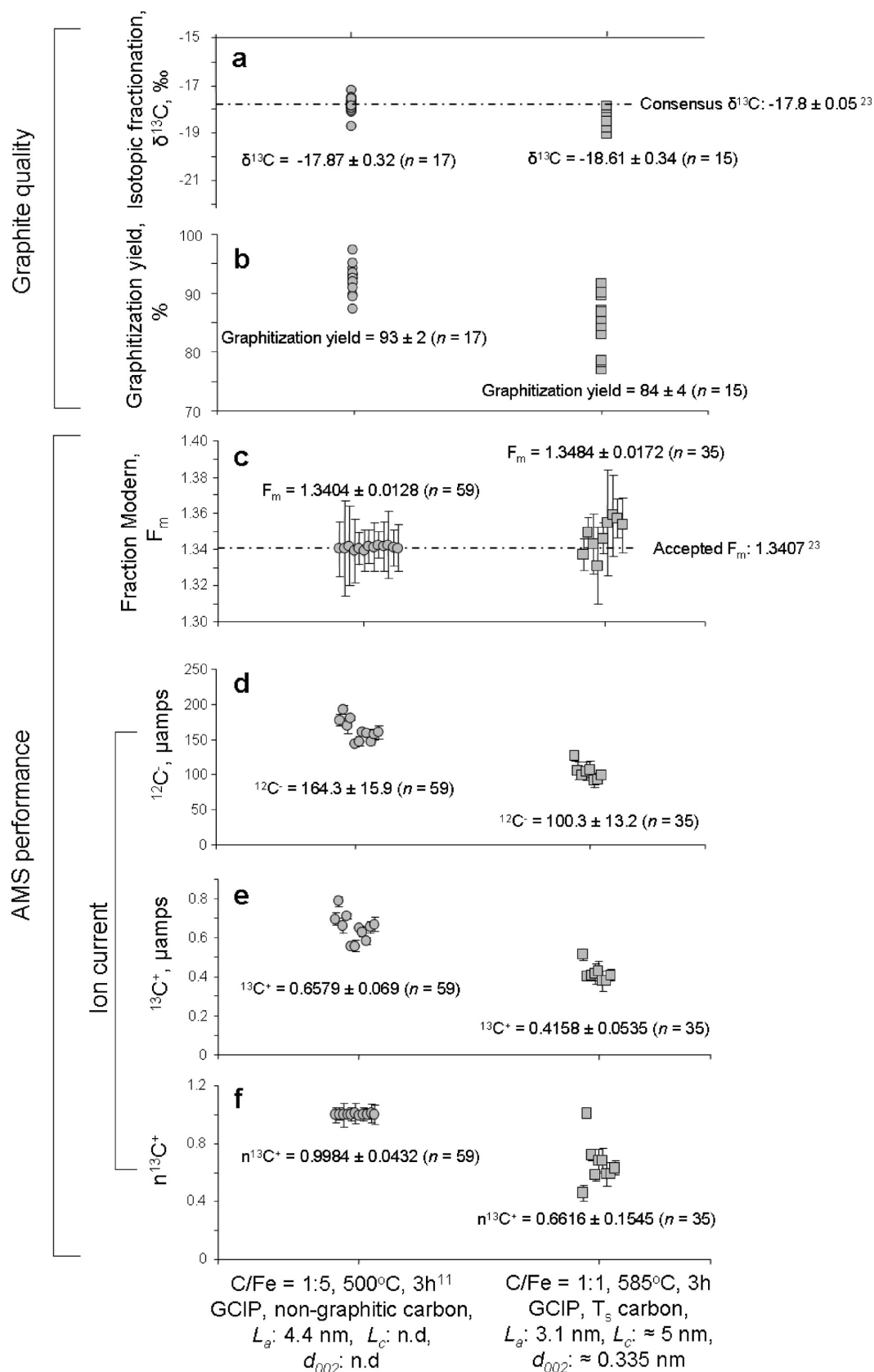


Figure 6. Comparisons of the isotopic fractionation ($\delta^{13}\text{C}$), graphitization yield, F_m (^{14}C level), and ion currents ($^{12}\text{C}^-$, $^{13}\text{C}^+$, $n^{13}\text{C}^+$) of the two AMS targets of GCIP with different graphite crystallinity. The AMS target of GCIP (C/Fe = 1:1, 585 °C, 3 h) had more ordered nanocrystalline graphite (T_s carbon, L_c ≈ 5 nm, d₀₀₂ ≈ 0.335 nm in Figure 2) than the AMS target of GCIP (C/Fe = 1:5, 500 °C, 3 h).¹¹ However, the AMS target of GCIP (C/Fe = 1:1, 585 °C, 3 h) had an ≈0.7‰ larger isotopic fractionation (Figure 6a), a 9% lower graphitization yield (Figure 6b), a less accurate and precise F_m (relative error = 0.5743%, Figure 6c), and an ≈40% lower $^{12}\text{C}^-$, $^{13}\text{C}^+$, and $n^{13}\text{C}^+$ currents (Figure 6d–f) than the AMS target of GCIP (C/Fe = 1:5, 500 °C, 3 h).¹¹ The $n^{13}\text{C}^+$ (Figure 6f) was unitless. The d₀₀₂ in the GCIP (T_s carbon) as measured by XRD was ≈0.335 nm, while the d₀₀₂ in the GCIP (T_s carbon) as measured by HRTEM (Figure 5e) was 0.342 nm.

tallite, or both. Furthermore, the d_{002} (0.3354 nm)³³ in graphite material also increased as the crystalline defect increased.¹⁸ Therefore, the a-C presented with no XRD pattern.¹⁹ The a-C did not convert to perfect graphite crystals even at high temperature (3000 °C) and high static pressure (15 GPa).^{31,32}

In the present study, the G-002 was found to be the AMS targets of GCIP with C/Fe ratio of 1:1 at 500, 525, and 585 °C. The intensity of G-002 was increased as temperature increased (Figure 2). Only the AMS target of GCIP with C/Fe ratio of 1:1 at 585 °C was measurable to d_{002} (≈ 0.335 nm) and L_c (≈ 5 nm). A prior study¹⁸ that used higher temperature (750 °C) and longer graphitization time (12–24 h) produced larger sized graphite crystal (L_c : 15–20 nm) than the present study. The remaining AMS targets of ICM, GCI, and GCIP in Figure 2 did not show the G-002 because they were not sufficiently crystalline. They contained a-C, disordered nanocrystalline graphite (<5 nm), small amount of (nanocrystalline) graphite, or a combination of all these three factors. The AMS target of ICM processed at 400 °C in Figure 2 did not show the G-002, because of methane production limiting graphite formation at lower temperatures (<500 °C).^{29,34}

Raman spectroscopy was very sensitive in determining the crystallinity (in-plane direction, 2D) of graphite because it detected changes in the polarizability as well as the symmetric/asymmetric vibrational energy. The Raman spectrum of well-ordered graphite had a weak D band at ≈ 1330 cm^{-1} (fwhm = ≈ 60 cm^{-1}), sharp/intense G band at ≈ 1560 cm^{-1} (fwhm = 15–30 cm^{-1}), and intense G' band at ≈ 2700 cm^{-1} (fwhm = 70–90 cm^{-1}).^{35–38} The D band was reported as a disorder-induced band, because it became more intense and broad as the crystalline defect in the graphite material increased.³⁹ Other disorder-induced bands (D' at ≈ 1620 cm^{-1} , D + G at ≈ 2950 cm^{-1}) also became more intense and broad as the crystalline defect in the graphite material increased.^{36,38,40} Crystalline defects also increased as the number of edge carbons in the graphite material increased.^{8,41}

Raman spectra of the AMS targets of GCIP (Figure 3b–e) had intense/broad D and G bands and weak/broad G', D + G, and D' bands that were similar to those of the C-Fe, glassy carbon, or soot.^{26,38,42} The L_a was small due to small surface area of Fe (C/Fe = 1:1, 1 mg each), even when the temperature was increased from 500 to 585 °C. In contrast, the L_c was large due to increase in the degree of stacking sequence caused by small surface area of the Fe (C/Fe = 1:1, 1 mg each), as the temperature increased from 500 to 585 °C (Figure 3c–e). The

AMS targets of GCIP (Figure 3b–d) contained nongraphitic carbon, while the AMS target of GCIP (Figure 3e) had T_s carbon, although the L_c in the AMS target of GCIP (Figure 3e) was a little smaller (≈ 5 nm) than common crystalline size (6–20 nm) of T_s carbon, (see Supporting Information, Figure S1). Thus, the AMS target of GCIP (Figure 3e) might have contained the C-Fe, nanocrystalline graphite sheet, a-C, and/or Fe_3C . Formation of well-ordered graphite crystal may be feasible with the C/Fe ratio of 1:1 at higher temperature (>2500 °C) using our HT Zn reduction method,¹¹ consistent with Figure 4b. However, a Raman spectrum of this graphite material might still appear with a weak D band, since the presence of the D band was reported in graphite material produced at 3000 °C.⁴⁰

HRTEM visualized crystal structure (including crystalline defects) of the graphite material at an atomic scale. Using the HRTEM, the present study characterized the carbon sheets and the presence of carbon-encapsulated Fe (C-Fe) in our two AMS targets of GCIP. We also found that carbon sheet was formed as the carbon shell was thickened in the C-Fe. As the temperature increased, the size of carbon sheet was enlarged and crystallinity of carbon sheet was also increased (Figure 5). In the present study, the HRTEM images of the C-Fe were consistent with prior studies;^{25–27} however, crystalline properties (crystal size and crystallinity) of the carbon shell in the C-Fe were different due to different graphitization conditions (i.e., Fe particle size, temperature, ratio of C/Fe etc.). Our HT Zn reduction method¹¹ was thermodynamically favorable for graphite formation, so it may be feasible to produce well-ordered graphite with a minor modification of our conditions¹¹ (i.e., temperature, time, etc.).

Graphite Quality versus ^{14}C -AMS Performance. Graphite is the standard sample format for ^{14}C -AMS measurement because it has minimum sample to sample contamination and produced a more reliable ion current than the CO_2 gas sample format.⁴ However, the graphite material can easily absorb aerosol or vapor contamination, so graphitization facilities need to be very clean.⁹

In general, accurate/precise/HT ^{14}C -AMS measurement must produce reliable ion current (C^- of >100 μA) from the target sample without differential isotope loss.⁴³ The AMS target should have good thermal conductivity to produce reliable ion currents.¹ The surface of AMS target was hot during ionization by the Cs^+ sputter, so cesium was absorbed and revaporized from the AMS target surface throughout the sputtering ionization process. Keeping more cesium on the AMS target surface raised the C^- current.^{17,44}

The Zn reduction method¹⁸ produced iron carbide or a mix of well-ordered graphite and poorly crystallite materials that produced $^{12}\text{C}^-$ of ≈ 7 μA . The mean $\delta^{13}\text{C}$ shift (-8%) from samples was variable to $\pm 4.0\%$.¹⁸ One method¹⁸ used 50–100 mg of zinc powder, 10–30 mg of iron powder, 10–30 mg of nickel foil, zinc at 400 °C, iron at 700–750 °C, nickel foil at 500–700 °C, and a duration of 12–24 h. The other Zn reduction method¹⁵ which used ≥ 40 mg of Zn powder, 10–40 mg of TiH_2 powder, a proper amount (not specified) of cobalt powder, at 500 °C for 3 h, and at 550 °C for 2 h produced graphite that yielded a $^{12}\text{C}^-$ of 30–60 μA . Graphitization yield was $\approx 80\%$,

- (30) Stanjek, H.; Häusler, W. *Hyperfine Interact.* **2004**, *154*, 107–119.
(31) Cheng, H. M.; Endo, H.; Okabe, T.; Saito, K.; Zheng, G. B. *J. Porous Mater.* **1999**, *6*, 233–237.
(32) Onodera, A.; Higashi, K.; Irie, Y. *J. Mater. Sci.* **1988**, *23*, 422–428.
(33) Chung, D. D. L. *J. Mater. Sci.* **2002**, *37*, 1475–1489.
(34) McNichol, A. P.; Gagnon, A. R.; Jones, G. A.; Osborne, E. A. *Radiocarbon* **1992**, *34*, 321–329.
(35) Ferrari, A. C.; Robertson, J. *Phys. Rev. B* **2001**, *64*, 075414.
(36) Escribano, R.; Sloan, J. J.; Siddique, N.; Sze, N.; Dudev, T. *Vib. Spectrosc.* **2001**, *26*, 179–186.
(37) Nikiel, L.; Jagodzinski, P. W. *Carbon* **1993**, *31*, 1313–1317.
(38) Knight, D. S.; White, W. B. *J. Mater. Sci.* **1989**, *4*, 385–393.
(39) Tuinstra, F.; Koenig, J. L. *J. Chem. Phys.* **1970**, *53*, 1126–1130.
(40) Pimenta, M. A.; Dresselhaus, G.; Dresselhaus, M. S.; Cañado, L. G.; Jorio, A.; Saito, R. *Phys. Chem. Chem. Phys.* **2007**, *9*, 1276–1291.
(41) Wang, H. M.; Wu, Y. H.; Choong, C. K. S.; Zhang, J.; Teo, K. L.; Ni, Z. H.; Shen, Z. *Nanotechnology* **2006**, *1*, 219–222.
(42) Sadezky, A.; Muckenhuber, H.; Grothe, H.; Niessner, R.; Pöschl, U. *Carbon* **2005**, *43*, 1731–1742.

- (43) Ognibene, T. J.; Bench, G.; Brown, T. A.; Peaslee, G. F.; Vogel, J. S. *Int. J. Mass Spec.* **2002**, *218*, 255–264.
(44) Ishikawa, J. *Nucl. Instrum. Methods Phys. Res. Sect. B* **2007**, *261*, 1032–1035.

and the mean $\delta^{13}\text{C}$ shift was -2.2% from the consensus $\delta^{13}\text{C}$ ($-10.8 \pm 0.5\%$) of the ANU.¹⁵ Some samples produced cobalt carbides that resulted in 5–10% measurement error in $^{14}\text{C}/^{13}\text{C}$ ratio due to lower ion currents.¹⁵

In the present study, the AMS target of GCIP (C/Fe = 1:1, 585 °C) contained more ordered nanocrystalline graphite compared to the AMS target of GCIP (C/Fe = 1:5, 500 °C). However, sample qualities of the AMS target of GCIP (C/Fe = 1:1, 585 °C) were not optimal for accurate/precise/HT¹⁴C-AMS measurement, because it had larger $\delta^{13}\text{C}$ shift, lower graphitization yield, less accurate/precise F_m , and lower ion currents (Figure 6).

Furthermore, the GST (L_a : 37.9 nm, L_c : 21.2 nm, d_{002} : 0.336 nm) and the AMS target of GCIP¹¹ (L_a : 4.4 nm, L_c : nondeterminable, d_{002} : nondeterminable) were also compared for accurate/precise/HT¹⁴C-AMS measurements (see Supporting Information, Figure S4). The AMS target of GCIP was produced from the GST using our HT Zn reduction method.¹¹ Although differences of graphite crystallinity between the AMS targets of GST and GCIP were significant ($P < 0.0001$), this difference did not affect the accurate/precise/HT¹⁴C-AMS measurements (see Supporting Information, Figure S4). The difference of F_m between the AMS targets of GST and GCIP was from background carbon during graphitization, not from graphite crystallinity.

The presence of Fe in the AMS target was found to contribute indirectly to the generation of C^- ion current. The present study found that the presence of Fe powder, which was used as a metal binder in the AMS targets, had a greater affect on C^- current than carbon type in the AMS targets. Previous workers had noted that carbon types like charcoal, natural graphite, or pyrolytic graphite affected C^- current produced by Cs^+ sputter.⁴⁵ The same study⁴⁵ noted that pyrolytic graphite deposited on tantalum wire yielded the best C^- ion current.⁴⁵ In the present study, the high thermal conductivity of Fe (as metal binder) favored retention of cesium on the carbon/graphite/Fe surface in the AMS target (minimizing cesium vaporization), which produced the intense C^- current.^{17,45} In addition, Fe (as catalyst) also increased the chemical reaction rate during graphitization.⁴⁶ In the present study, 1 mg of Fe (C/Fe = 1:1) produced a more ordered crystalline graphite than 5 mg of Fe (C/Fe = 1:5). On the other hand, the C/Fe ratio of 1:1 was kinetically less favorable in converting CO_2 (1 mgC) to graphite in 3 h. Therefore, an optimum C/Fe ratio, a longer graphitization time, and/or a higher graphitization temperature were required to form ordered crystalline graphite, complete the graphitization reaction, and minimize the $\delta^{13}\text{C}$ shift. Hence, despite different carbon types in AMS targets, a greater amount of Fe powder as catalyst and metal binder (C/Fe = 1:5) in AMS targets provided better thermal conductivity, guaranteed the production of reliable C^- current (140 $\mu\text{A}/\text{mgC}$), high graphitization yield (93%), and small $\delta^{13}\text{C}$ shift which led to accurate/precise/HT¹⁴C-AMS measurements.

The C/Fe ratio of 1:5 produced the AMS target of GCIP that was superior to that of the 1:1 C/Fe ratio. Although the AMS target of GCIP^{8,11} had nongraphitic carbon, the higher surface area from 5

mg Fe powder (C/Fe = 1:5) had lighter $\delta^{13}\text{C}$ shift of 0.07%, higher graphitization yield ($93 \pm 2\%$), and a better thermal conductivity, which collectively produced accurate/precise/HT¹⁴C-AMS measurements (Figure 6). The combination of higher CO_2 reduction temperature (585 °C) and larger C/Fe ratio (1:1) increased graphite crystallinity (T_s carbon, $L_c \approx 5$ nm, L_a : 3.1 nm, $d_{002} \approx 0.335$ nm). The smaller surface area from the 1 mg of Fe powder resulted in the lighter $\delta^{13}\text{C}$ shift of 0.81%, 9% lower graphitization yield, and lower thermal conductivity, which led to lower ion currents or less accurate/precise F_m .

CONCLUSION

Graphitization yield and thermal conductivity of AMS targets were more important factors for accurate/precise/HT¹⁴C-AMS applications than the carbon type. However, carbon type (graphite crystallinity) can still play a role. Although the iron carbides may be acting as the catalyst for formation of graphite (Figure 4), increasing the amounts of iron carbides (i.e., Fe_3C) in AMS targets was detrimental for ¹⁴C-AMS measurement due to its physical traits (very hard solid) and $\approx 15\%$ lower ion currents compared to graphite or graphite-like materials in AMS targets. There is need for further work to determine the role of iron carbides in catalytic formation of graphite. Our results are important for accurate/precise/HT¹⁴C-AMS applications for in vivo human ADME and PBPK of nutrients, drug candidates, phytochemicals, and environmental samples.²²

ACKNOWLEDGMENT

The authors thank the reviewers for their perceptive and helpful comments. This work was supported by NIH DK-078001, DK-081551, DK-45939, DK-48307, and the USDA Regional Research W-143 from the California Agricultural Experiment Station. Raman spectra were made at the Spectral Imaging Facility of the NEAT-ORU, Chemistry Department, UC Davis supported by NSF-MRI-DMR-0723118 and NSF-MRI-DMR 0421521. Graphitization yield and isotopic fractionation was measured by Dr. David Harris at Stable Isotope Facility, Plant Science Department, UC Davis. Aspects of this work were performed under the auspices of the U.S. Department of Energy by Lawrence Livermore National Laboratory and supported by the Office of Science, Office of Basic Energy Sciences, Division of Materials Science and Engineering under contract DE-AC52-07NA27344 and NIH National Center for Research Resources Grant RR13461. This work was supported in part by the Office of Science, Office of Basic Energy Sciences, Division of Materials Sciences and Engineering, of the U.S. Department of Energy under Grant Number DE-FG02-03ER46057. The authors appreciated Professor Haiyan Wang and Mr. Joon Hwan Lee at Texas A&M University and Michael Dunlap at UC Merced for fruitful discussion on HRTEM measurement. Authors thank Professor Nilesh W. Gaikwad at UC Davis for reviewing the semifinal manuscript.

SUPPORTING INFORMATION AVAILABLE

Additional information as noted in text. This material is available free of charge via the Internet at <http://pubs.acs.org>.

Received for review September 15, 2009. Accepted February 3, 2010.

AC9020769

(45) Hedges, R. E. M.; Wand, J. O.; White, N. R. *Nucl. Instrum. Methods* **1980**, *173*, 409–421.

(46) Chang, R. *Physical Chemistry for the Biosciences*, 3rd ed.; University Science Books: Herndon, VA, 2005.